2018

Biomechanical Stability of Intraarticular Fractures of the Distal Femur Fixed by Intramedullary Nailing

Christian T. Davis
Lehigh University, ctd217@lehigh.edu

Biomechanical Stability of Intraarticular Fractures of the Distal Femur Fixed by Intramedullary Nailing

by

Christian Davis

A Thesis

Presented to the Graduate and Research Committee

of Lehigh University

in Candidacy for the Degree of

Master of Science

in

Mechanical Engineering

Lehigh University

August 2018

Certificate of Approval

This thesis is accepted and approved in partial fulfillment of the requirements for the Master of Science.

_____

Date

_____

Thesis Advisor, Dr. Hannah Dailey

_____

Chairperson of Department, Dr. Gary Harlow

Table of Contents

List of Tables

List of Figures

Abstract

Intramedullary (IM) nailing is a common fixation procedure for fractures of the distal femur (thighbone). These injuries are commonly associated with older individuals, and aging population demographics present the need to investigate IM nailing procedures for distal femur fracture fixation in osteoporotic bone. Accordingly, the goal of this study was to develop a mechanical testing fixture and protocol to assess the stability of distal femur fractures treated by IM nailing, including fracture models with and without metaphyseal comminution, and further investigate synthetic surrogate bone materials to best mimic osteoporotic bone for mechanical testing. This work describes the design and development of a testing fixture and loading protocol that mimicked the anatomic and mechanical loading scenarios of the femur while additionally providing a non-interfering bearing surface during mechanical testing. Results from axial loading tests indicated that for intraarticular distal femur fractures with moderate bone quality, a total subsidence (or permanent deformation resulting in fixation collapse) of 4-5 mm may occur. The potential implications of this subsidence may be relevant for construct selection in a clinical setting. Separately, ASTM-standard materials tests were carried out on materials identified as potential candidates to serve as homogeneous substitutes for metaphyseal bone. Polyurethane foam blocks of three different densities were tested and the results compared with reported relationships between age and mechanical properties of bone in the distal femur. These findings suggested that outside of severe osteoporosis, a 15 lb/ft^3 density foam may most accurately represent the clinically relevant bone for future testing utilizing synthetic materials. Further investigation into *in vivo* bone quality of distal femur fracture patients may support improved synthetic material selection.

Introduction

Distal femur fractures have historically comprised about 3-6% of all femoral fractures[1–3]. Younger patients may sustain this type of injury due to a high-energy trauma and are more likely to have metaphyseal comminution[4]. However, the distribution of patients with distal femur fractures is often described as bimodal, skewed toward high-energy injury in young males and low-energy injury in older females[2,4,5]. This observation is supported by recent epidemiological data suggesting that distal femur fractures should be considered predominantly an osteoporotic injury dominated by older females[3]. Accordingly, the prevalence of these injuries may be expected to significantly increase with the shifting demographics of the aging population in the next 20-30 years[3].

Surgical management options for distal femur fractures include plating and nailing constructs. Nailing has recognized advantages compared to plating, such as high construct strength, less soft tissue disruption, a centralized axis of loading to promote earlier weight bearing, uniform mechanical stimulation, and symmetric callus formation[4,5]. Early retrograde nails were indicated for extra-articular fractures only, but application to fractures with articular involvement has been enabled by the recent introduction of certain advantageous design features in commercially available implant systems, including compact distal screw configurations to capture short condylar segments and fixed-angle constructs achieved via locking end caps[4]. However, the stability achieved by retrograde IM nailing depends upon the quantity and quality of available bone, and for this reason some authors still conservatively recommend locking plates in cases with short distal fragments or intraarticular comminution[6].

For implant systems designed with multiplanar distal fixation for robust purchase in poor quality bone, the central question is whether the construct can withstand early mobilization without substantial loss of reduction or subsidence requiring revision. Several previous biomechanical investigations have used cadaver and synthetic tissue models in destructive testing to assess construct stability and strength, some with particular attention to the challenges of fixation in osteoporotic bone[1,7,8]. However, these studies have been limited to extraarticular[1,8–15] and simple intraarticular osteotomy fracture models[7,8,16].

Accordingly, this study had three central objectives. First, to develop a repeatable test method for assessing the mechanical stability of distal femur fractures fixed by retrograde intramedullary (IM) nailing. Second, to assess whether distal femur fractures with metaphyseal comminution can be effectively stabilized by retrograde IM nailing with multiplanar distal fixation. Third, to investigate the most appropriate synthetic osteoporotic bone material for use as a low-cost, high-repeatability alternative to cadaver tissues.

Materials and Methods

Femoral Constructs: Bone Models

Synthetic femurs, comprised of 22 lb/ft^3 closed cell polyurethane foam were purchased from Sawbones (Pacific Research Laboratories, Inc., Vashon, WA, USA). Femur density was determined in-house by massing the femurs using a digital scale and calculating volume from a scanned model. All femurs were anatomically left to permit the use of anatomically left testing fixtures. The femurs themselves were of uniform

density, with no change in properties throughout the femur to delineate between cortical and trabecular/cancellous bone. Although composite synthetic bones have an established history of use and validated mechanical properties for the femoral shaft[17], bone in the distal femur is predominantly cancellous and homogenous foams have been previously proposed as biomechanical test materials to mimic the mechanical properties in this region[7].

Femoral Constructs: Sample Preparation

The synthetic femurs were prepared for testing through a four-step process: cutting, drilling, osteotomy, and fixation. The synthetic femurs received from SawBones were full-length femurs, and as such were cut down using a table saw to leave only a 90 mm portion of the distal end. Using a 3D-printed drilling guide (Figures 1, 2), the guide holes for the transverse and oblique locking screws were precisely drilled into the distal femur samples.

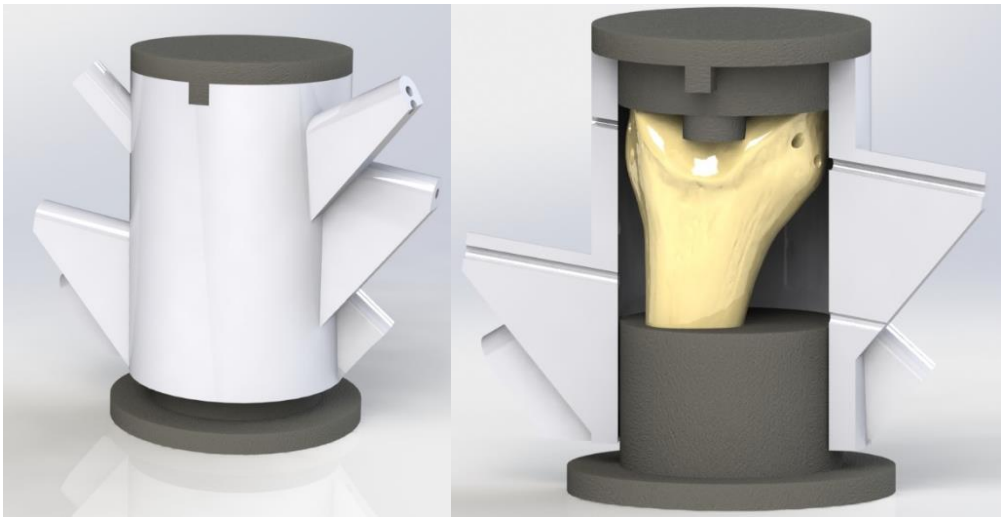

Figure 1: Rendering of SolidWorks (Dassault Systemes SolidWorks Corporation, Waltham, MA, USA) model of 3D-printed drilling fixture. The distal femur sample is compressed between two plungers (black) at a known location with the cylindrical body. A drill bit is then guided through the branches of the cylinder to precisely aim the drill holes.

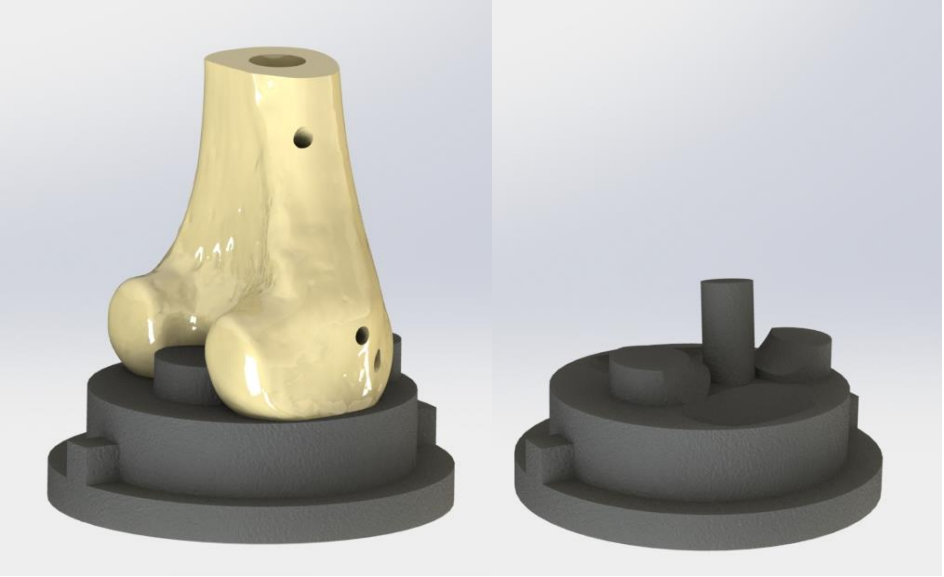

Figure 2: Rendering of SolidWorks (Dassault Systemes SolidWorks Corporation, Waltham, MA, USA) model of base for 3D-printed drilling fixture. The distal femur sample can be seated on the base of the fixture to ensure a reproducible drilling angle.

Following drilling, osteotomy fracture models were created to represent AO/OTA intraarticular distal femur fractures with and without metaphyseal comminution (Figure 3).

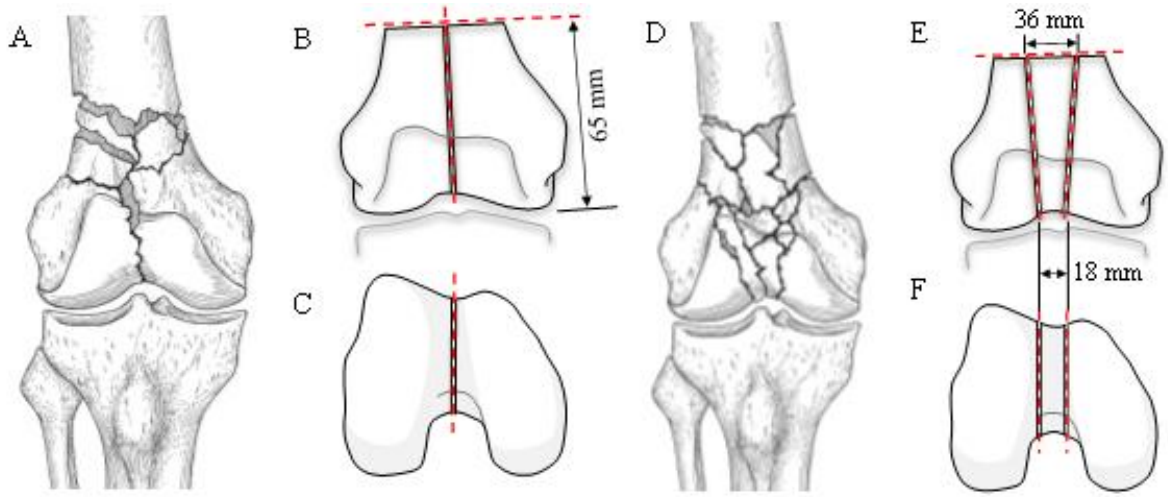

Figure 3: Two osteotomy fracture models were used. (A-C) AO/OTA 33-C2 fractures with diaphyseal comminution and a 65mm distal segment. (D-F) AO/OTA 33-C3 fracture with diaphyseal and metaphyseal comminution, represented by a 2:1 trapezoidal osteotomy with distal aspect match to the width of the intracondylar notch[18]. Red dashed lines indicate jig-guided osteotomies. Panels (A) and (D) are adapted from Gwathney *et al.*[19].

To facilitate the osteotomy of the distal femur samples, two additional 3D-printed fixtures were utilized (Figure 4). Using a scroll saw with a 0.36 mm thick blade (Skip Tooth, 11.5 TPI 44800, The Olson Saw Company, Bethel, CT, USA), each femur sample was appropriately osteotomized to cut a 37 mm proximal segment from the sample and to make cuts representing the fracture lines for the OA/OTA 33-C2 or OA/OTA 33-C3 fracture types. The fixtures served as a guide to direct the cutting operations.

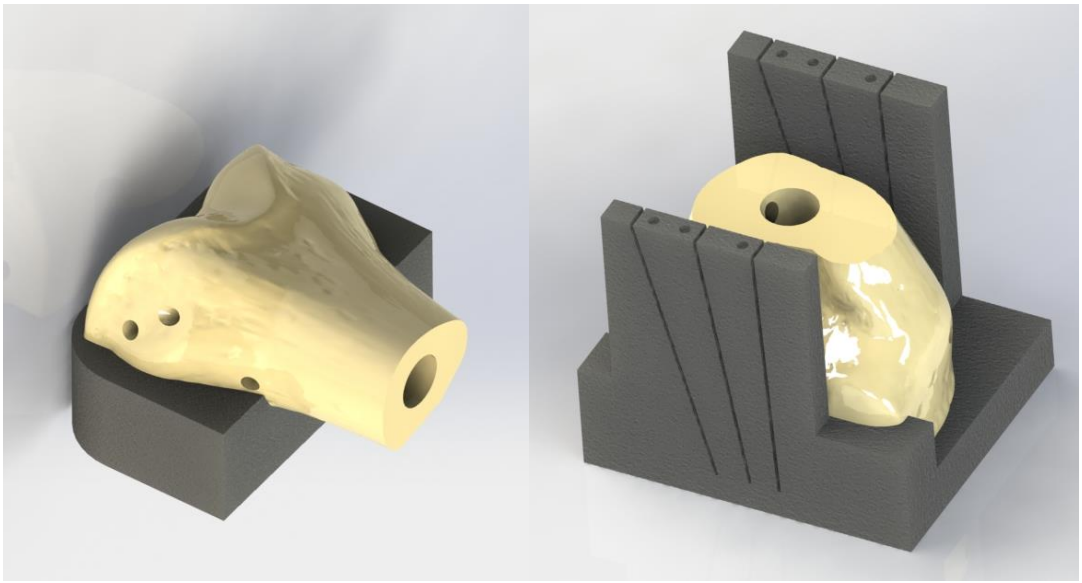

Figure 4: Rendering of SolidWorks model of 3D-printed cutting fixtures and distal femur sample. Using the guide-slots in the fixture, a scroll saw is used to osteotomize the fixture according to the prescribed fracture type (AO/OTA 33-C2 or AO/OTA 33-C3).

Finally, each distal femur sample, now drilled and osteotomized to reflect either an AO/OTA 33-C2 or AO/OTA 33-C3 fracture (Figure 1) was stabilized using a reference prototype femoral IM nailing system (OrthoXel, DAC; Cork, Ireland). Distal segments were fixated by hand using two oblique locking screws and one transverse screw (Figure 5). Proximal locking was executed using two anteroposterior locking screws. The fully assembled system was then set aside to wait for mechanical testing (Figure 6).

Figure 5: Representative orientation of distal locking screws. Distal locking was achieved through the use of two oblique locking screws and one transverse screw.

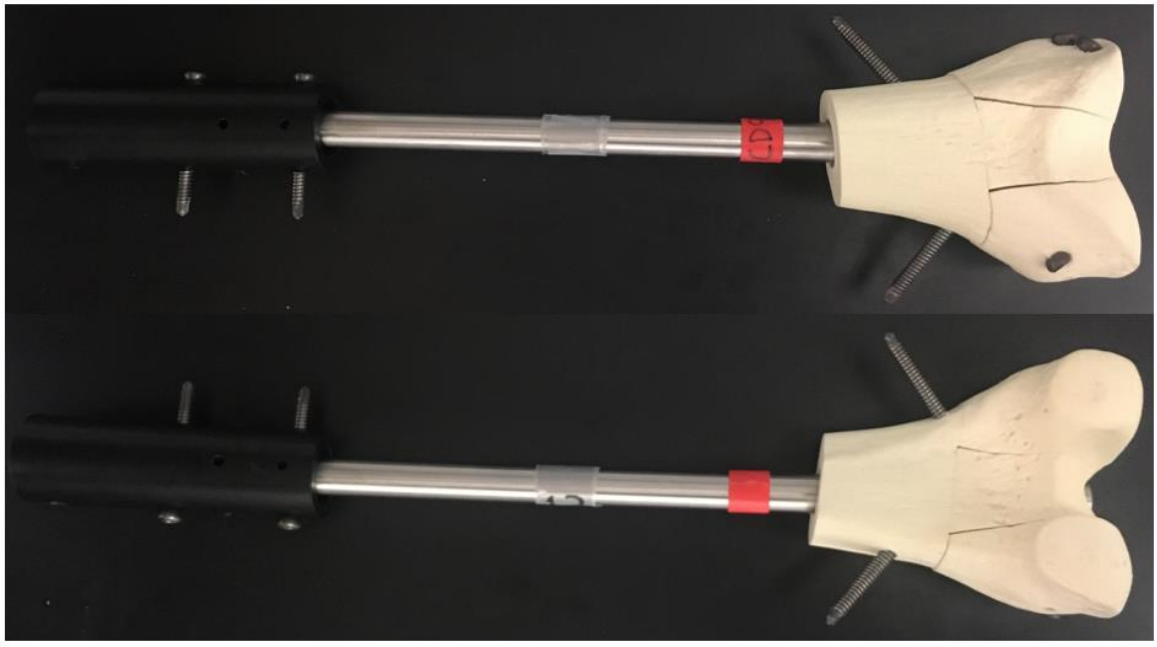

Figure 6: Anterior (top) and posterior (bottom) views of fully assembled construct of a distal femur fracture with metaphyseal comminution. The excessively long oblique screws would not be used in clinical practice, as this would cause soft tissue irritation and dysfunction, but do not change the mechanical performance of the construct when loading according to the procedure described herein.

Femoral Constructs: Mechanical Testing

All testing for synthetic distal femur fracture models was carried out on a Zwick multi-axis material testing machine (Zwicki Z5.0TN, Zwick/Roell, Kennesaw, GA, USA) with a 5 kN axial load cell and 20 N-m torque cell. The test fixture was designed to accommodate both torsional and axial loading modes, provide a highly-repeatable alignment of the anatomic axis of the femur, minimize point contacts between the distal fragments and tibial bearing surface, and mediate relative free motion of the distal fragments during axial loading (Figure 7).

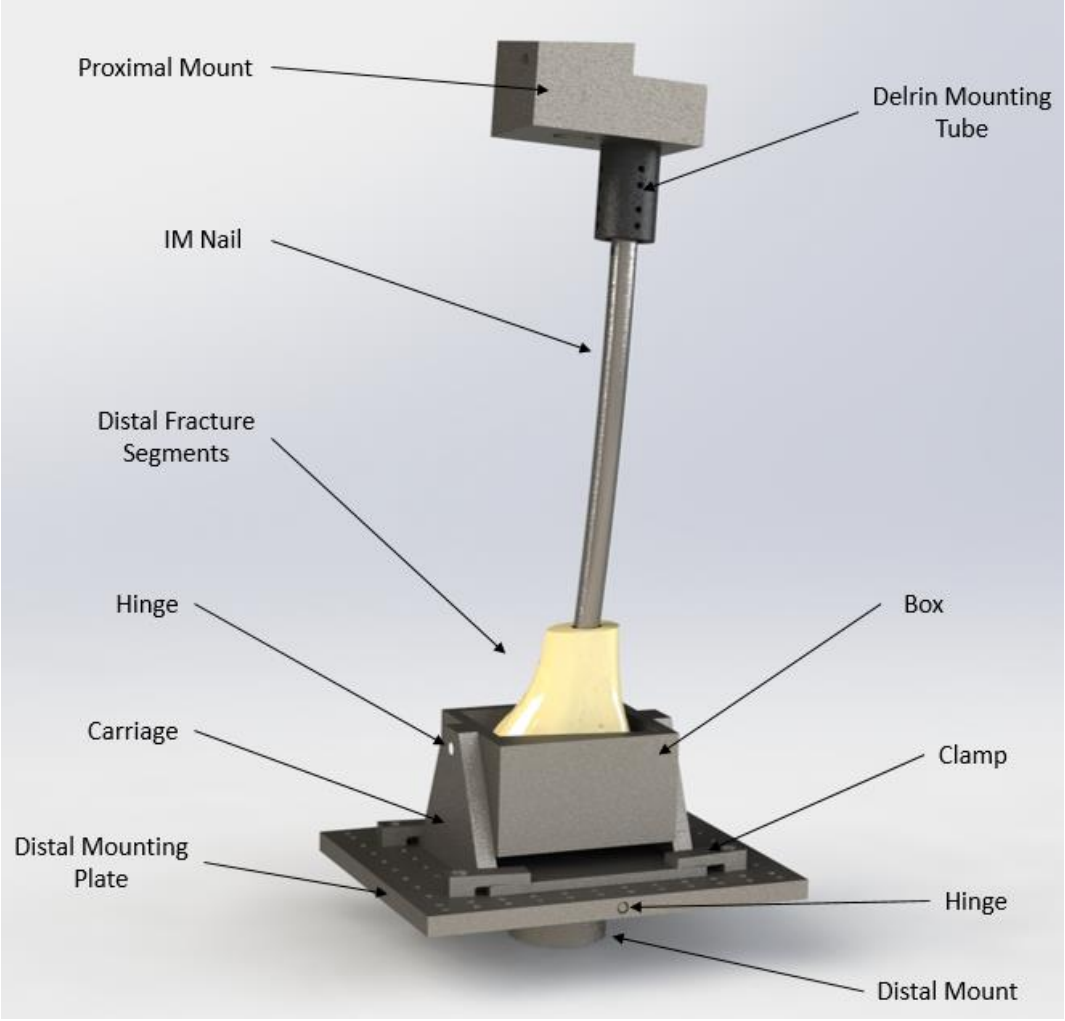

Figure 7: SolidWorks rendering of test fixture for multiaxial loading with proximal mount designed for high repeatability alignment of anatomic axis

The *proximal mount* of the test fixture (Figure 7) was designed to align the mechanical axis of the full femur (Figure 8) with that of the testing machine. Accordingly, measurements were taken from a scan of the synthetic femurs acquired from SawBones (Pacific Research Laboratories, Inc., Vashon, WA, USA), which detailed a loading angle of 6.40 deg, an angle of posterior tilt of 7.90 deg, and an angle of anteversion of 23.24 deg. In doing so, the proximal mount permitted the IM nail and fixated distal fragments to consistently contact the center of the distal portion of the fixture as defined by the loading axis of the testing machine.

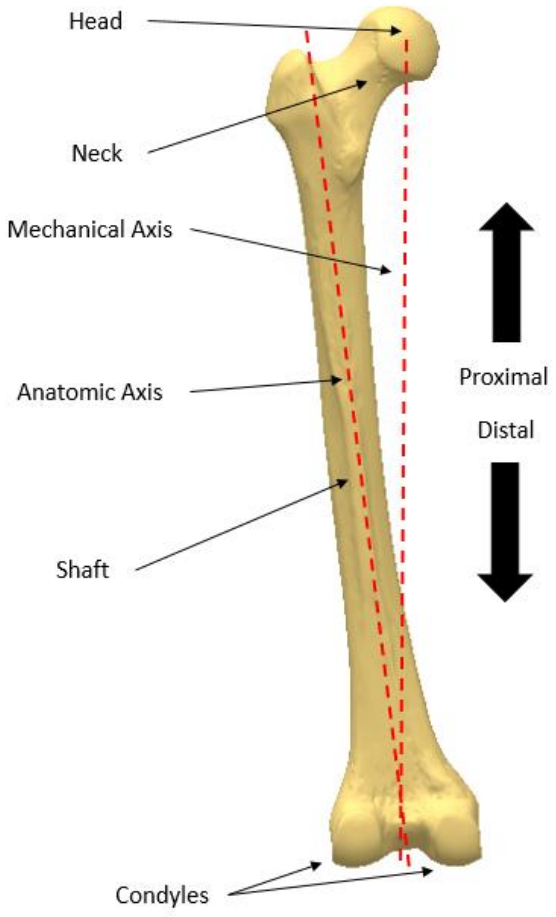

Figure 8: Anatomic representation of left femur displaying anatomic and mechanical loading axis', proximal and distal directions, and major features. Femur pictured is scan of femur model used in testing.

The distal portion of the fixture comprised a modified universal joint (cardanic mount), providing two rotational degrees of freedom with respect the loading axis of the testing machine. The second degree of freedom of the cardanic mount was achieved through a hinged *box*, into which the distal fragments sat. The box could be additionally translated freely in the plane of the *distal mounting plate* to find the natural center of each specimen and thereby reduce residual forces associated with inconsistencies in the biomechanical axis of the nail and fracture with respect to the loading axis of the testing machine.

Figure 9: Test fixture for multiaxial loading with proximal mount designed for high repeatability alignment of anatomic axis

Inside the box, the synthetic distal femur rested on a high-density polyethylene (HDPE) custom-machined insert (Figure 10), which was designed to precisely mirror the geometry of the bearing portion of the femoral condyles as determined from the provided scan. The selection of HDPE as the insert material matched that of tibial tray inserts commonly used in knee-replacement procedures. Previous investigators have sought to use these tibial trays as the fixture bearing surface[1,7], however in doing so have introduced points contacts between the distal fragments and the tibial bearing surface during testing. The goal of conforming the bearing surface to the shape of the test sample was to reduce the prevalence of these point contacts, thereby providing a more physiologically representative testing environment and minimizing sample compression due to high loads.

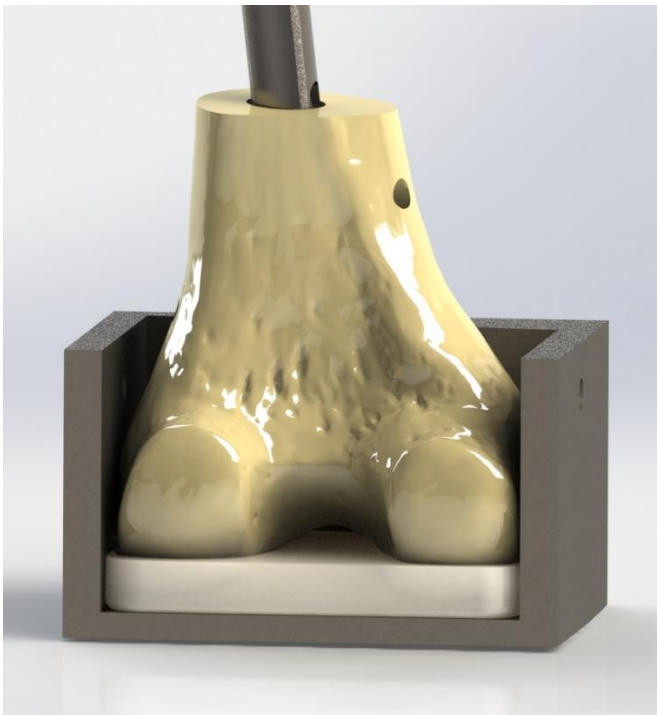

Figure 10: Section view of testing fixture box to show HDPE custom machine insert

Fracture models were subjected to non-destructive torsional testing followed by destructive axial testing. The non-destructive torsional testing was carried out at across a torque range of ± 5 N-m, corresponding to a torque value between the upper limit (mean plus standard deviation) observed for "at rest" sitting and supine poses with an instrumented femoral implant[20] and the upper limit (mean plus standard deviation) observed clinically in static partial weight bearing[20], while still remaining within the expected range for normal slow gait[21]. Torsion testing was conducted for five complete cycles to exclude run-in effects at a rate of 18 deg/min[22,23] and with a 20 N static axial compressive preload to maintain engagement with the tibial bearing surface[7].

Axial testing was conducted using a stepwise incremental destructive loading protocol based on the work of several previous investigators[1,7,9,13–15]. Under zero torque, cyclic compression oscillated from 20 N to 200 N, at a maximum loading rate of 6 mm/s. After every 500 cycles, the minimum and maximum loads were increased by 10 N and 100 N, respectively. Testing was continued until construct failure, defined as an observed subsidence of greater than 5 mm (determined by crosshead travel of the test machine), or catastrophic failure of the distal fragments of the implant.

Polyurethane Foam: Synthetic Bone Materials

Tests of fracture fixation mechanical stability have historically used cadaveric and synthetic bone-mimetic materials such as polyurethane foams. The disadvantage of cadavers is the attendant risk and costs and a lack of standardization due to variations in individual anatomy and bone quality that makes comparisons between different types of fixation challenging. Given that one of the purposes of this investigation was to develop

a repeatable test method, synthetic bone-mimetic foam was identified as the material of choice for the experimental test.

Three grades (densities) of closed cell polyurethane foam, 10 lb/ft^3, 15 lb/ft^3, and 20 lb/ft^3 were chosen for evaluation. The choice of these three foam grades came as a result of the match between the reported compressive strengths for the given grades[24] and the reported range of compressive strength for cancellous bone in the older population[25]. This relationship can be seen below in Table 1 and Figure 11 below. Grade 10 foam was selected so as to provide comparison with Wähnert *et al.*[7], while grades 15 and 20 were chosen to represent foams with compressive strengths mostly commonly seen in the older adult and elderly population. Foams were purchased from Sawbones (Pacific Research Laboratories, Inc., Vashon, WA, USA) in the form of rectangular blocks (130mm x 180mm x 40mm) in which the rise of the foam was controlled through the 40mm thickness of the block. The foam blocks were later machined into consistently sized samples for compression testing.

Grade	Minimum Compressive Strength [MPa]	Maximum Compressive Strength [MPa]
5	0.4495	0.7800
10	1.745	2.820
12	2.485	3.970
15	3.820	6.050
20	6.630	10.45
25	10.15	16.00
30	14.30	22.70
35	19.15	30.55
40	24.60	39.55
50	37.35	61.05

Table 1: "Requirements for Compressive Strength" from ASTM F1839

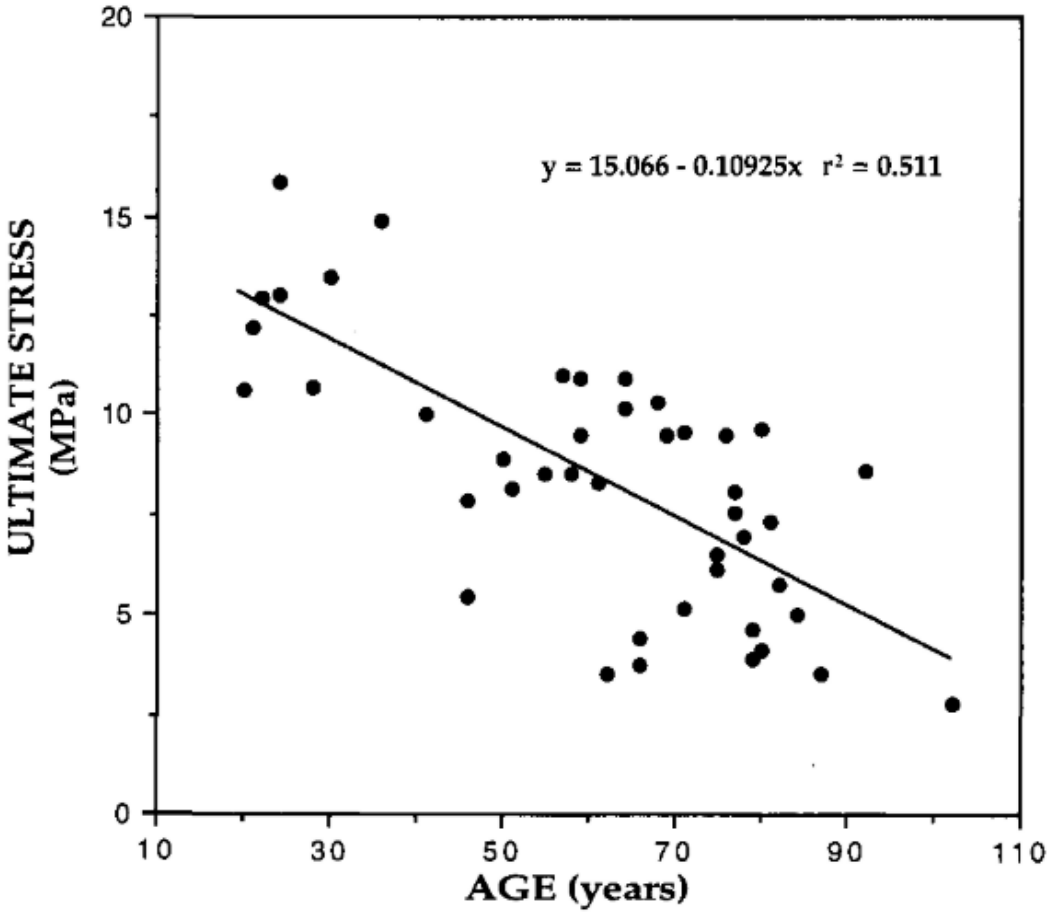

Figure 11: Ultimate compressive stress of cancellous bone samples as a function of donor age, reproduced from McCalden *et al.* (1997)[25]

Polyurethane Foam: Sample Preparation

The polyurethane foam blocks were preparing according to ASTM standards F1839 and D1621[24,26]. Using a facing mill and table saw, each foam block was machined into six rectangular samples, 50.4 mm x 50.4 mm x 25.4 mm. Each sample was measured post-process to ensure accurate dimensioning. Following machining, the density of each sample was determined according to ASTM D1622[27] by volumetric measurement of each block using calipers and massing of each block using a digital scale.

Polyurethane Foam: Mechanical Testing

The polyurethane foam blocks were tested using an Instron single axis material testing machine (Instron 5567, Instron Engineering Corporation, Norwood, MA, USA) with a 30 kN axial load cell. The blocks were tested according to ASTM F1839[24], which subsequently prescribed the used of ASTM D1621 for compressive testing[26]. As such, each sample was compression tested at a rate of 2.54 mm/min (10% of overall height per minute) until deformation of 3.3 mm was achieved (13% of overall height). Compression testing utilized a standard compression platen to support the bottom of each sample, and a flat ¼ inch steel plate on the top of each sample to evenly distribute the compressive load applied by the machine crosshead during testing.

For testing of the polyurethane foam, a sample size of six blocks was chosen. This is consistent with ASTM D1621, which requires a minimum sample size of five from which to determine compressive modulus[26]

Results

Femoral Constructs: Torsional Testing

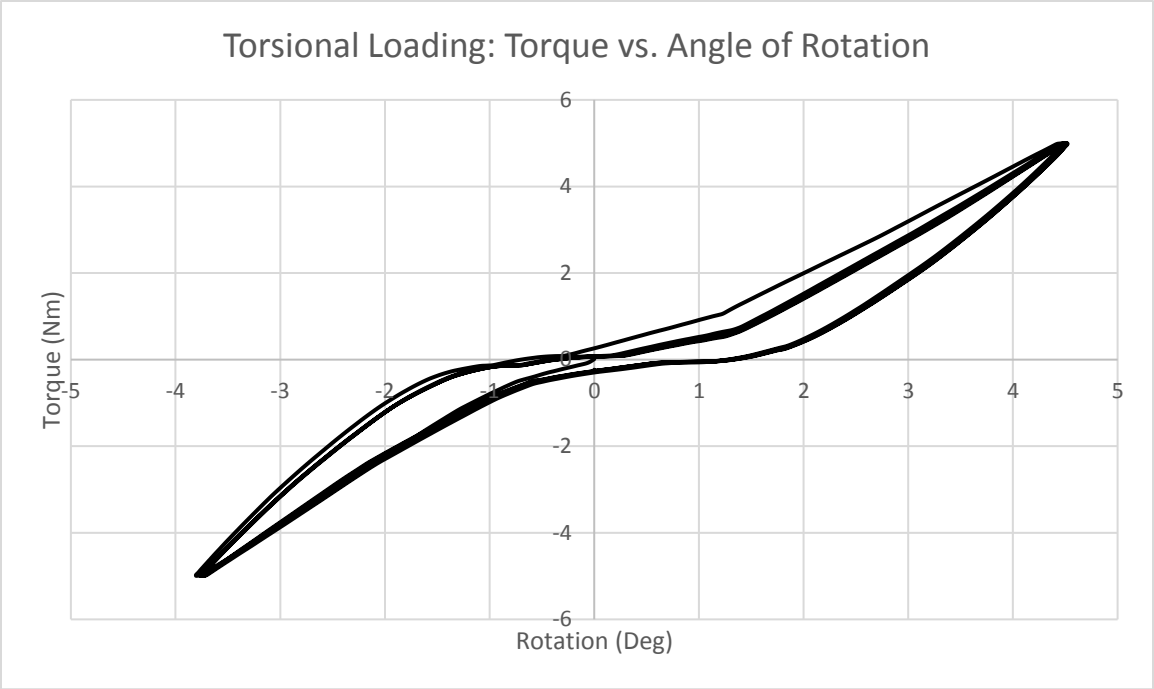

Figure 12: Torque vs. angle curve for sample NC3 (without metaphyseal comminution). Representative of torque-angle curves seen for each sample

Torsion testing was carried out prior to axial destructive testing. A standard torque-angle curve can be seen above in Figure 12. Comparing across fracture types, constructs without metaphyseal comminution displayed an average torsional stiffness of 1.15 ± 0.08 N-m/deg, while constructs with metaphyseal comminution displayed an average torsional stiffness of 1.35 ± 0.19 N-m/deg (Figure 13). Utilizing a two tail two sample equal variance t-test, a p-value of 0.095 was achieved, indicating a non-statistically significant difference between the two sets of torsional stiffness values.

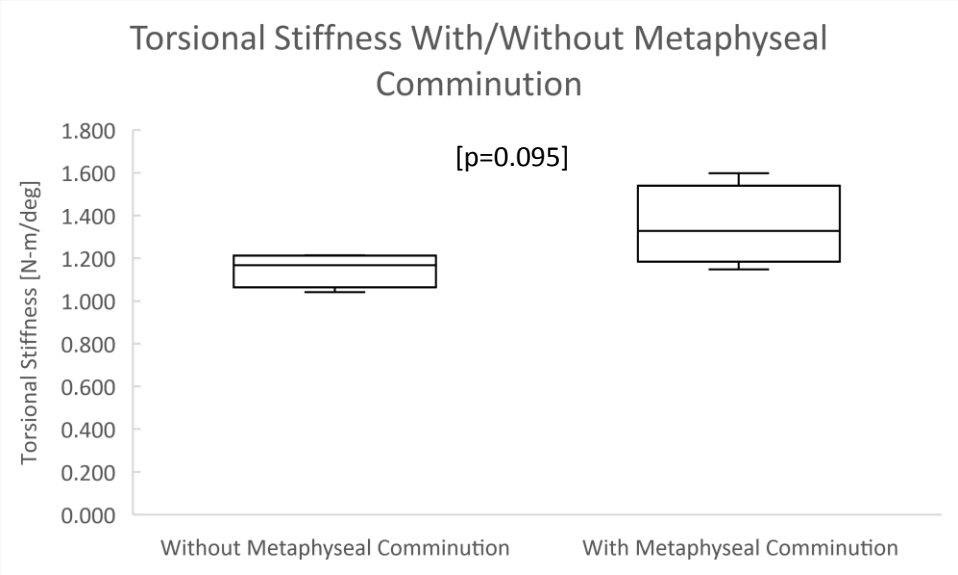

Figure 13: Torsional stiffness of constructs with and without metaphyseal comminution. Constructs subject to torque test of range ±5 N-m at a loading rate of 18 deg/min (N=4 per group).

Femoral Constructs: Axial Testing

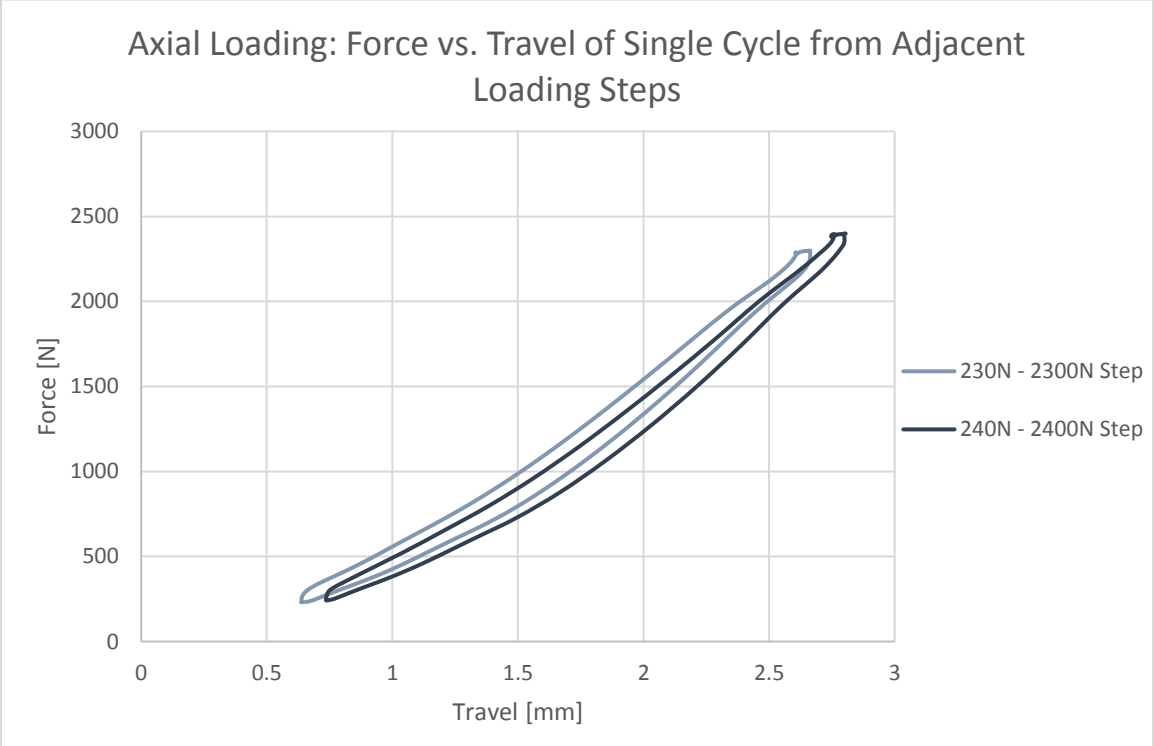

Figure 14: Standard axial loading curve displaying force vs. travel for a single cycle from the 230N – 2300N and 240N – 2400N loading steps for NC4 (without metaphyseal comminution).

A standard axial loading curve displaying force vs. travel for a single cycle of two subsequent loading steps can be seen above in Figure 14. During the axial destructive testing, the axial stiffness was measured during the last cycle of each 500-cycle loading step. For the first loading step (20N – 200N), the average axial stiffness for constructs without metaphyseal comminution was 763 ± 52.6 N/mm. For constructs with metaphyseal comminution it was 671 ± 28.0 N/mm (Figure 15). The decrease in axial stiffness for constructs with metaphyseal comminution as compared to those without was statistically significant at a p-value of 0.021.

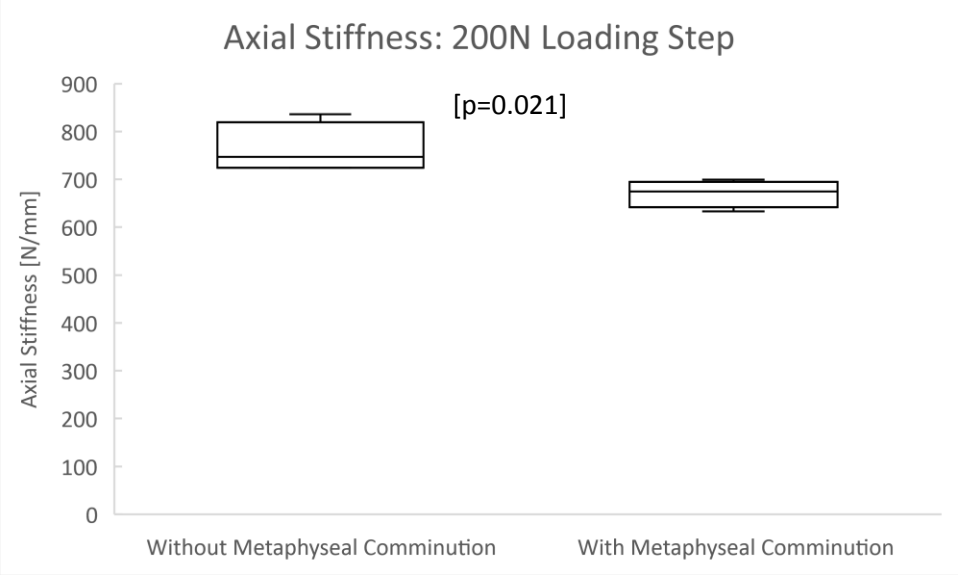

Figure 15: Axial stiffness of construct as measured during the first loading step (N=4 per group).

For the 3000N loading step, which represented the largest magnitude loading step for which all constructs shared a full 500 cycles of data, the average axial stiffness of constructs without metaphyseal comminution was 1140 ± 33.3 N/mm, and the average axial stiffness of constructs with metaphyseal comminution was 1050 ± 27.6 N/mm

(Figure 16). The decrease in axial stiffness for constructs with metaphyseal comminution as compared to those without was again statistically significant, with a p-value of 0.005.

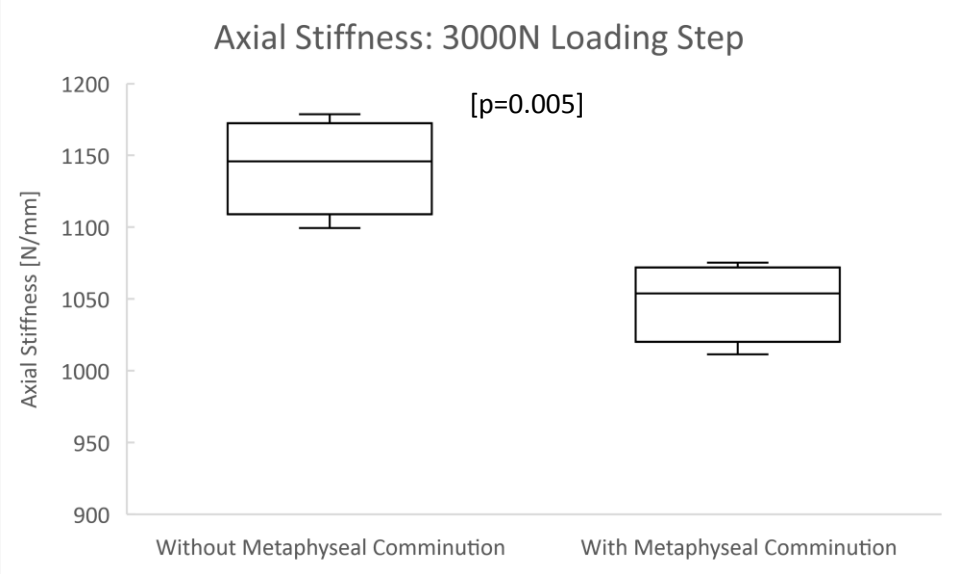

Figure 16: Axial stiffness as measured during 3000N maximum force loading step (N=4 per group).

For each construct, the maximum crosshead travel at each loading step is seen below in Figure 17. Orange-hued data points indicate samples with metaphyseal comminution and blue-hued data points indicate samples without metaphyseal comminution.

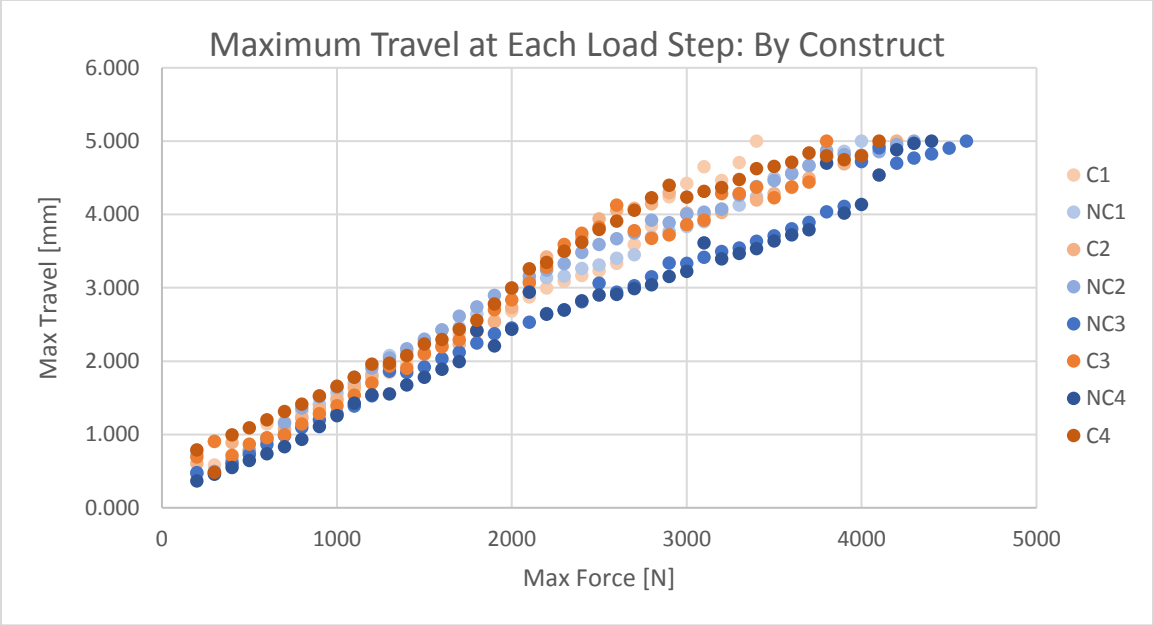

Figure 17: Maximum travel at each load step, by construct

To further investigate the rate of subsidence of each fracture type, data from Figure 17 was combined into two groups: maximum travel at each loading step for constructs with metaphyseal comminution and maximum travel at each loading step for constructs without metaphyseal comminution. Figure 18 displays these two groups alongside the linear best fit of each group. When reported this way, the data suggests that the presence of metaphyseal comminution increased the rate of subsidence under axial loading compared to cases without metaphyseal comminution.

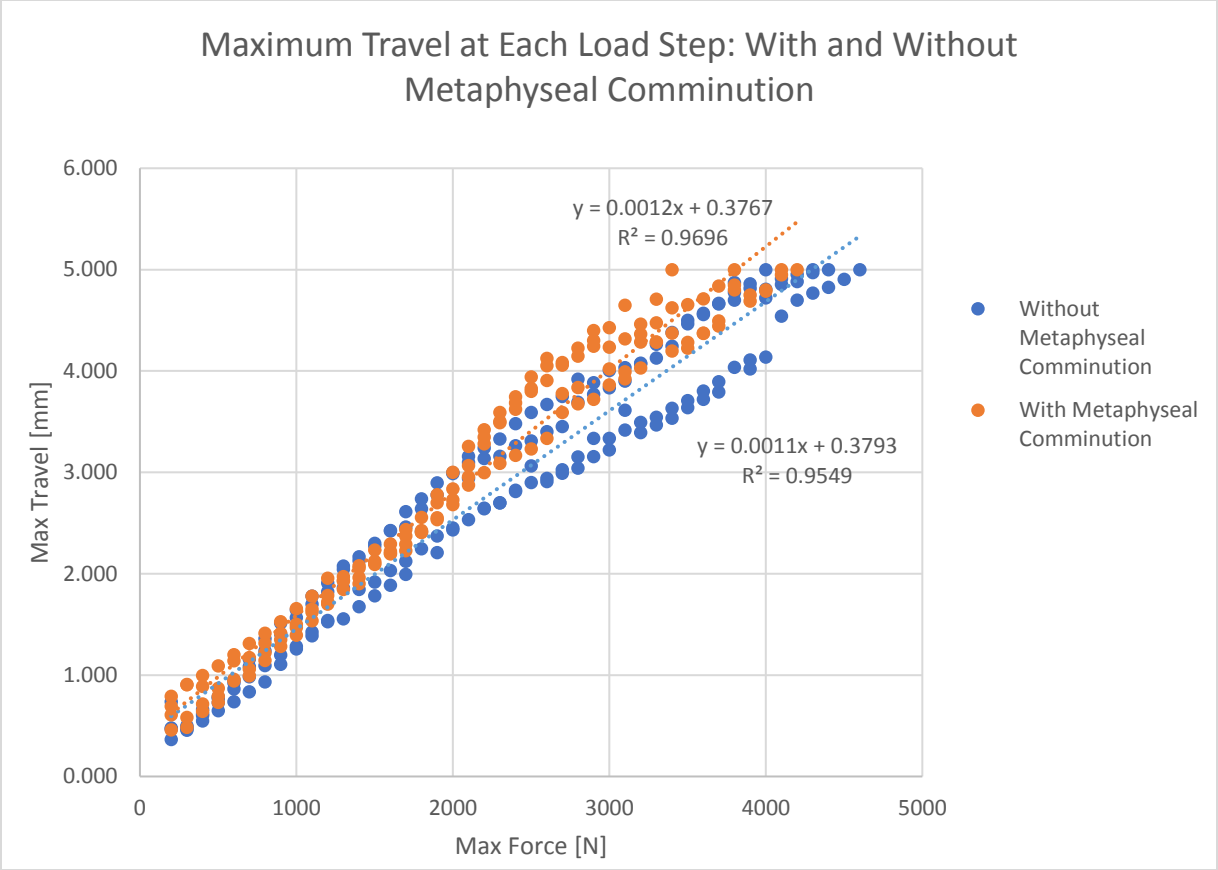

Figure 18: Maximum travel at each load step, by group

To best quantify the rate of subsidence of a construct under axial loading, the maximum travel at each loading step was determined for each sample. A linear regression was fit to the load-step travel data, with the slope of this linear best fit representing the change in subsidence of the construct as a function of the maximum force of each loading step. Figure 19 below displays this rate of subsidence for constructs with and without metaphyseal comminution. The average rate of subsidence for constructs with metaphyseal comminution was 1.26 ± 0. 070 μm/N, and the average rate of subsidence for constructs without metaphyseal comminution was 1.10 ± 0. 070 μm /N. The increase in rate of subsidence for constructs with metaphyseal comminution as compared to constructs without is statistically significant with a p-value of 0.0168,

confirming the indications of the data represented in Figure 18, that the presence of metaphyseal comminution within the fracture resulted in an increased rate of subsidence.

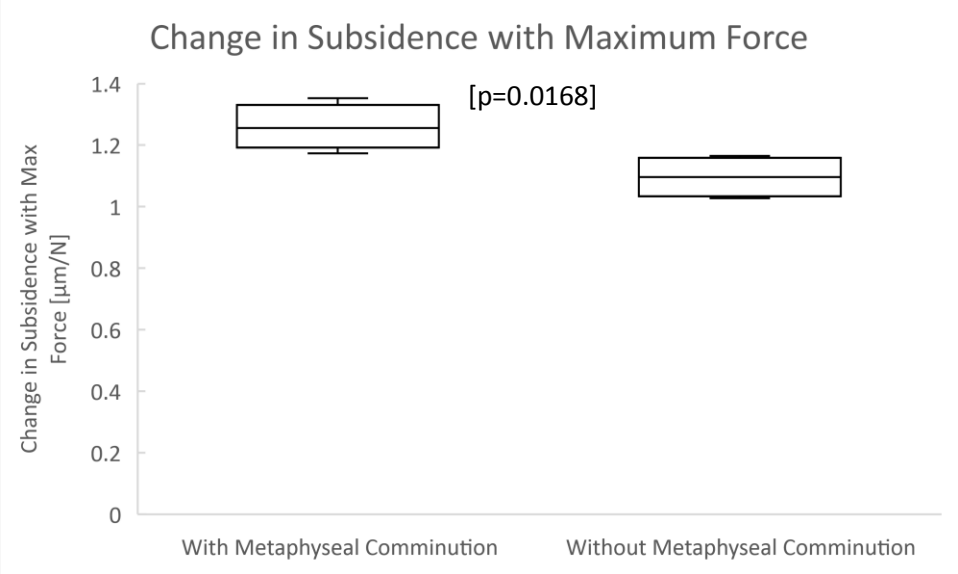

Figure 19: Change in subsidence with change in maximum force of loading step. Slope of the best fit line of the max travel vs. max force graph for each construct (N=4 per group).

Shifting to an investigation of failure, construct failure for this study was defined as subsidence of 5 mm at any point during an axial loading step. Based on this definition, the average cycles to failure for constructs with and without metaphyseal comminution are seen below in Figure 20. For constructs without metaphyseal comminution, the average cycles to failure was 20,000 ± 2,420 cycles, and for those with metaphyseal comminution it was 18,500 ± 1,800 cycles. While there was an observed decrease in cycles to failure in comparing constructs with metaphyseal comminution to those without, it was not statistically different at the current sample size of n=4.

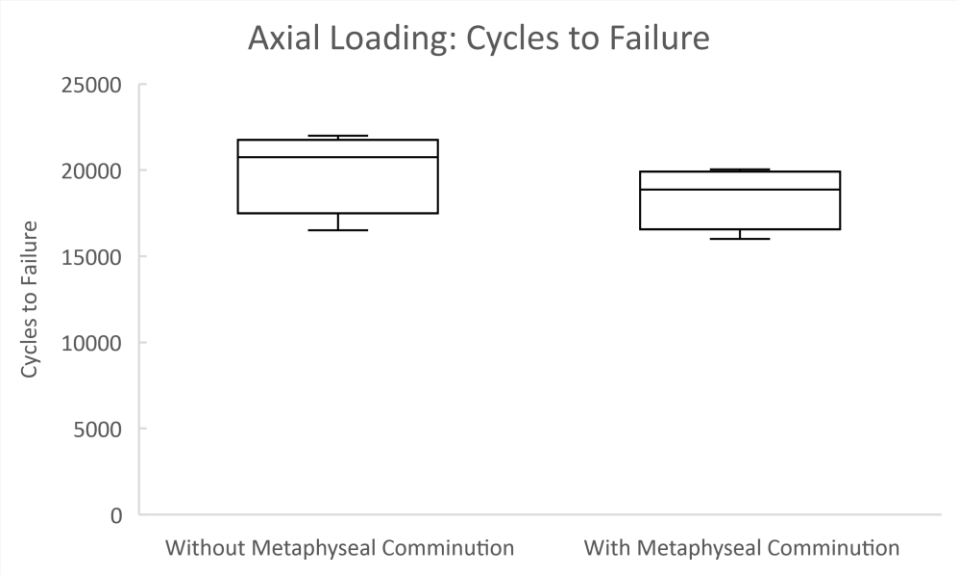

Figure 20: Cycles to failure, with and without metaphyseal comminution (N=4 per group).

To investigate the net subsidence of the fracture, the maximum crosshead travel for each cycle within the 300N – 3000N loading step for sample C2 (with metaphyseal comminution) can be seen (Figure 21). In the context of this figure the net travel, or net subsidence, is indicative of the irreversible deformation of the fracture. The 300N – 3000N loading step represents a general trend seen throughout all loading steps of the study, with much of the net travel of a loading step occurring within the early cycles of that loading step. For the loading step displayed in Figure 21, 41% of net subsidence of the loading step occurred within the first 10 cycles, and 81% of net subsidence occurred within the first 100 cycles, out of a total 500.

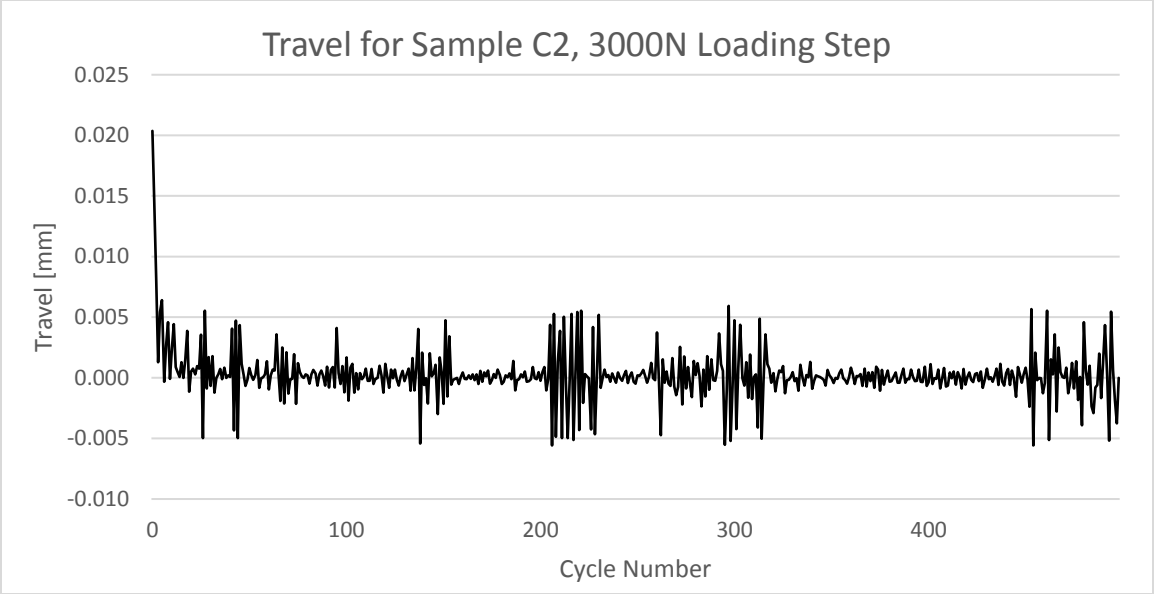

Figure 21: Representative subsidence curve for the 3000N loading step for sample C2. For this sample, 41% of the observed subsidence (permanent compression) occurred in the first 10 cycles and 81% of travel occurred within the first 100 cycles.

Subsidence of the titanium locking screws within the synthetic bone was observed in all samples and is exemplified below in Figure 22. Before and after images of sample C3 (with metaphyseal comminution) show elongation of the screw holes due to axial loading and the beginnings of crack propagation through the foam from the screw holes.

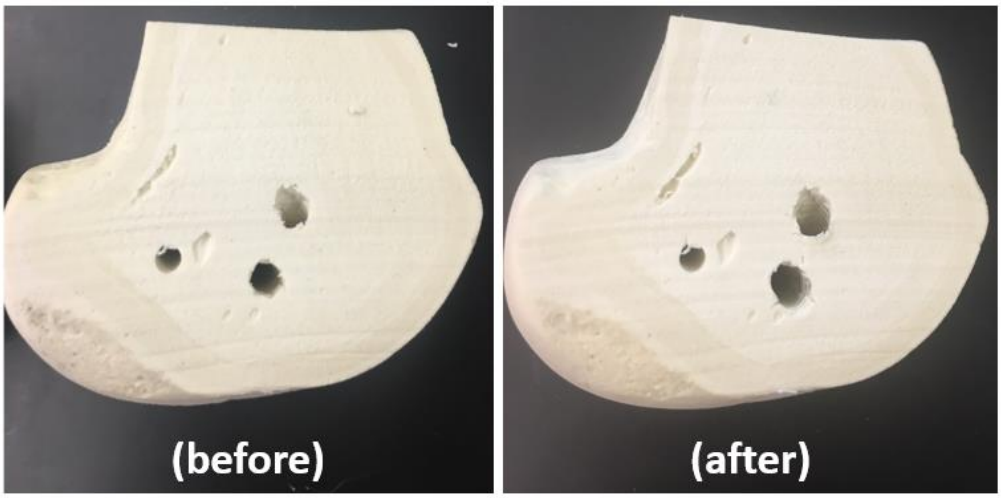

Figure 22: Before testing (left) and after testing (right) images of the cross section of the lateral portion of sample C3 (with metaphyseal comminution) following destructive axial loading. Elongation and crack propagation can be seen within the screw holes of the sample.

Polyurethane Foam: Compressive Testing

In compressive testing of the polyurethane foam samples, two values were measured: Compressive modulus and ultimate compressive stress. The compressive modulus for each foam sample can be seen below in Figure 23, with values of compressive modulus serving to determine compliance of the foams with respect to ASTM F1839: Standard Specification for Rigid Polyurethane Foam for Use as a Standard Material for Testing Orthopaedic Devices and Instruments.

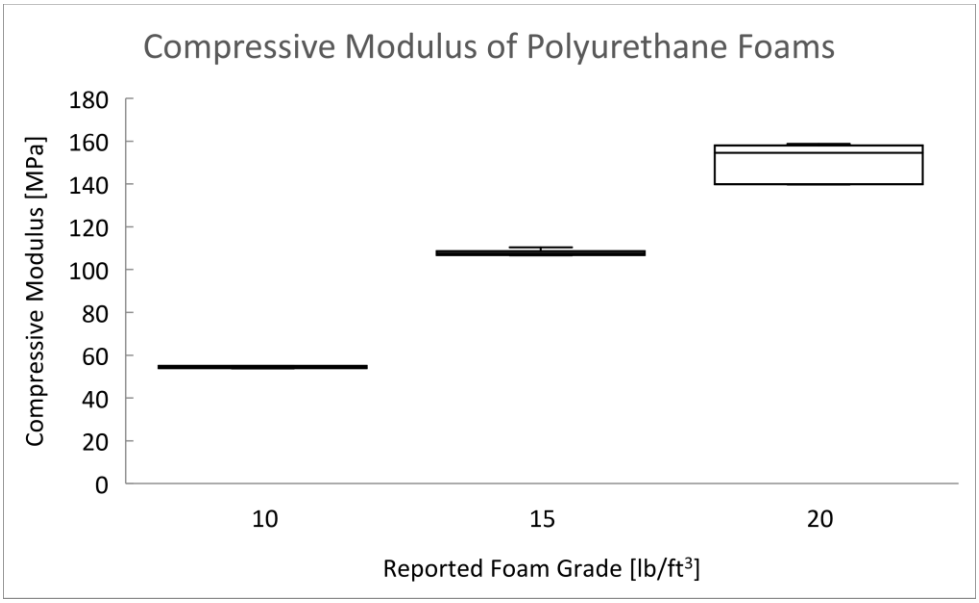

Figure 23: Compressive modulus of polyurethane foams samples from SawBones Inc. tested according to ASTM D1621

The above chart reports compressive moduli values of 54.4 ± 0.5 MPa, 107.8 ± 1.4 MPa, and 150.0 ± 9.4 MPa, for foams of grade 10, 15, and 20, respectively. Of the three densities of polyurethane foam tested, the 20 lb/ft^3 foam did not display a compressive modulus within the range defined by ASTM Standard F1839-08 (Table 2),

thereby resulting in classification as an ungraded foam, not to be used as a standard material for testing of orthopaedic devices.

Grade	Minimum Compressive Modulus [MPa]	Maximum Compressive Modulus [MPa]
5	12.30	20.35
10	45.75	71.70
12	64.50	100.5
15	98.00	151.0
20	167.5	2575.5
25	253.5	390.0
30	355.5	548.5
35	472.0	723.0
40	603.0	941.0
50	907.5	1435

Table 2: "Requirements for Compressive Modulus" from ASTM F1839

The ultimate compressive stress of the polyurethane foam samples can be seen below in Figure 24.

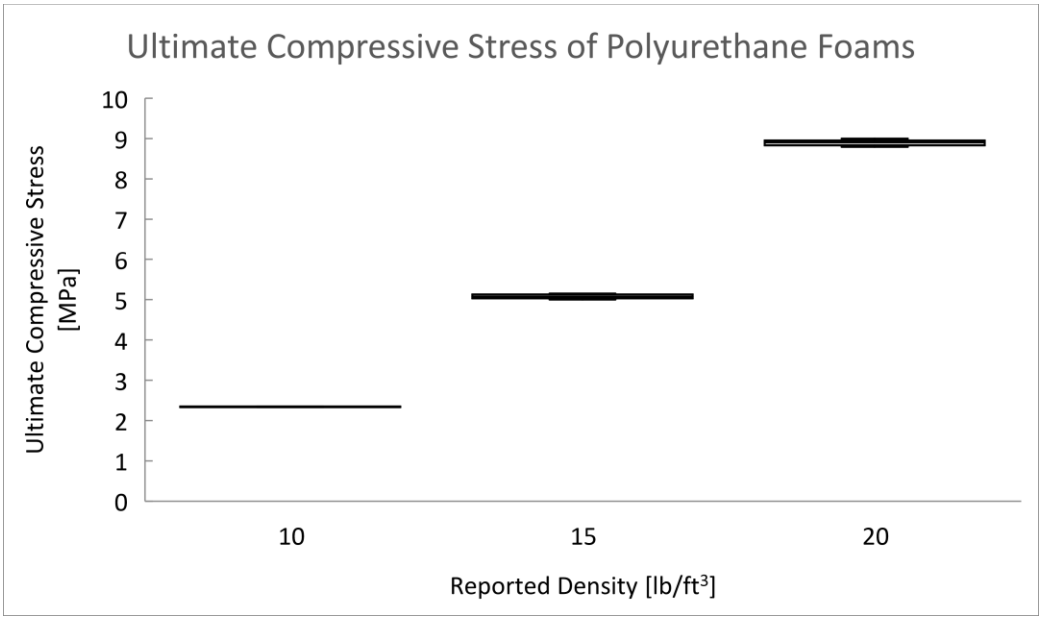

Figure 24: Ultimate compressive stress of polyurethane foams samples from SawBones Inc. tested according to ASTM D1621

The average ultimate compressive stresses of grades 10, 15, and 20 foams were 2.34 ± 0.008 MPa, 5.08 ± 0.054 MPa, and 8.89 ± 0.075 MPa, respectively. Comparing these average ultimate stresses to the age-related mechanical properties regression equation in Figure 11, the selected foams corresponded to approximate donor ages of 116, 91, and 56 years old, respectively[25].

Discussion

Comparing mechanical testing results across constructs with and without metaphyseal comminution, both axial stiffness and rate of subsidence results indicate that intraarticular fractures with metaphyseal comminution are less stable than those without. At both early and late loading steps within the axial testing regime, the axial stiffness of constructs with metaphyseal comminution was less than the axial stiffness of constructs without comminution. Additionally, the rate of subsidence was higher in constructs with metaphyseal comminution as compared to those without, indicating an earlier loss of reduction for intraarticular fractures with metaphyseal comminution. While the axial testing results indicate a difference in mechanical robustness between fractures with and without metaphyseal comminution, they do not indicate whether this difference affects the ability for fractures with metaphyseal comminution to be effectively stabilized with retrograde IM nailing. Rather, that determination is left to the clinical community to determine what level of construct robustness is necessary for successful healing outcomes.

From a clinical perspective, there is a clear need to address the question of whether immediate load-bearing is recommended in the early stages of recovery for intraarticular fractures of the distal femur treated with retrograde IM nailing. Within this study, the observed linear relationship between the maximum force applied in each axial loading step and the overall subsidence of the construct demonstrates an increase in subsidence with an increase in the maximum loading force. Additionally, much of the subsidence that occurred in each 500-cycle loading step was observed within the first 10-100 cycles of that stop. As such, using the linear best fit for fractures with metaphyseal

comminution, total subsidence for full weight bearing is estimated at 4.4 mm, assuming a total weight bearing value of 2.5 times bodyweight[28] for a 300 lb individual. Since the majority of subsidence is seen early in a loading step, the total subsidence should occur early within full weight bearing. Accordingly, if several millimeters of subsidence early in fracture healing is deemed not detrimental to overall recovery, then immediate load-bearing in the early stages of fracture recovery may be acceptable, with the expectation that new bone will begin to form, and that subsidence will be naturally self-limiting. Alternatively, if several millimeters of subsidence early in fracture healing is deemed negative to the overall recovery process, then a non-loading bearing regimen should be recommended in the early stages of fracture recovery.

While polyurethane composite femur models have previously been shown to display similar mechanical characteristics to that of healthy cadaver femurs[29], there has been little success in matching the mechanical characteristics of polyurethane foams with that of osteoporotic femurs. In investigating foams to imitate the properties of osteoporotic bone, the grade, or density of the foam has been shown to affect the subsidence of the resulting construct under a given load. Comparing the results of this study, which utilized polyurethane foam fracture models of density 22 lb/ft^3, to that of Wähnert *et al.*[7], which utilized a polyurethane foam of density 10 lb/ft^3, construct failure, defined as subsidence of 5 mm, was seen much earlier in the Wähnert study (4,000-7,000 cycles vs. 15,000-20,000 cycles in this study). It is important to note, however, that subsidence as defined in the Wähnert study was maximum travel of the test machine crosshead while applying a 190 N axial load, whereas subsidence as defined in this study was maximum crosshead travel observed at any point during axial testing, which

occurred over a range of loads, often much higher than 190 N. The inspiration for this definition of subsidence within the Wähnert paper comes due to the early catastrophic failure of many of their femoral constructs, thereby allowing for a low load of 190 N to induce 5 mm of subsidence.

With such disparity across the mechanical behavior of polyurethane foams of different densities, there is a need to determine what grade of foam most accurately represents osteoporotic bone. Wähnert *et al.*[30], sought to justify their selection of a very low density foam through qualitative means, but a more robust quantitative method is needed. Utilizing a relationship between the ultimate compressive stress and age of cancellous bone[25], the ultimate stress values obtained from the foam block compressive testing data allow for approximation of representative patient ages. Accordingly, the polyurethane foam samples of grades 10, 15, and 20, correspond to approximate patient ages of 116, 91, and 56 years, respectively. These approximations are consistent with expectations, with catastrophic failure of grade 10 foams indicating bone quality that may be too poor for an approximation of even osteoporotic bone[1]. As such, with grade 20 foam indicated a patient age of 56, which is representative of the older adult population but not of the age group most commonly associated with osteoporosis, further testing utilizing fractures of grade 15 foam is recommended.

In addition to this, with a marked lack of characterization of distal femur bone quality within the literature, and with the majority of mechanical properties of human bone derived from post-mortem samples[31–35], there is a need to characterize bone material properties for *in vivo* distal femurs, specifically for patients who have experienced distal femur fractures. In the future, this could be accomplished computationally using pre-

operative computerized tomography (CT) scans. This data would be useful for selection of appropriate homogenous foam models specifically tailored to match the mechanical properties of the distal femur in patients who experience the injury of interest.

In addition to these materials selection considerations, the test fixture for axial/torsional loading was designed with care to recreate a physiologically representative bearing surface for the distal end of the femur. To avoid spurious forces arising from sample alignment artifacts, the distal fixture was designed to allow tilting of both the coronal and sagittal planes through the use of a universal joint[1,7]. To model the interaction between the distal end of the femur and the knee joint, several methods of contact have previously been used in test fixtures. One method involves potting the entire distal portion of the femur in a material such as bone cement[13,15]. This method of interaction provides rigid fixation of the distal portion of the femur, which is not physiologically representative of the contact interface between the femur and the tibial tray (an interface most notably defined by interaction with the condyles). Furthermore, the purpose of this study was to investigate fracture in this region, which would be unnaturally fused by the potting approach. Previous authors have incorporated tibial tray inserts from total knee replacement procedures as bearing surfaces for the distal femur[1,7]. The limitation of this approach is that these tibial trays are designed to interact with specifically-sized and manufactured replacement femoral condyles, so the interaction with the distal portion of an anatomically accurate femur is non-ideal and consists of many point contacts, particularly in early testing. Accordingly, inspiration for the test fixture used in this study was drawn from Wild *et al.*[14], in using a custom machined block

of a low-friction material to provide a bearing surface that matches the condyles of the femur being tested as closely as possible.

While effort has been made in the design of this fixture to minimize point contacts between the femoral condyles and tibial tray during axial loading scenarios, there is still progress to be made in creating a more physiologically representative fixation system for torsional loading. As was the case in several previous studies[1,7], the test fixtures used for these experiments provided a non-anatomic mechanical interference between the distal bearing box fixture and the anterior and posterior surfaces of the distal femur during torsion testing. This fixture was effective in measuring the torsional stiffness of the construct without requiring any soft tissue constraints but created point contacts between the test fixture and the distal femur under torsional load. However, unlike the axial tests, torsion tests were not performed cyclically to failure, so these point contacts were not observed to produce progressive localized damage.

It is important to note the differences between the sequences of events in creation and treatment of a naturally occurring fracture versus that of the fracture generated in a laboratory setting. In contrast to naturally occurring fractures, which are irregular and irreproducible, the laboratory osteotomies created here were highly regular and consistent within groups. However, the notable disadvantage of the osteotomy fracture model is that the fracture pattern is created via a cutting operation, which must therefore produce a certain amount of material removal due to the cutting blade eating away at the material being cut. Accordingly, in the context of this study, the effect of this material removal was minimized by first drilling the guiding screw holes, so that the fixated fracture segments would maintain their original spatial relationship with one another once the

screws were inserted. The resulting fracture gaps were closed as much as possible between fracture segments, and although some minor variances in gap closure were observed qualitatively, these did not appear to introduce substantial variations in mechanical stability within groups.

One of the objectives of this investigation was to design a test method for assessing the mechanical stability of distal femur fractures, which was successfully achieved and now sets the stage for future work. For this future work, the current data suggests several opportunities for improvement, in addition to further investigation of synthetic bone materials. First, although clear trends were observed that would indicate differences between the two fracture patterns considered, these did not rise to the level of statistical significance across all assessment criteria due to the limited sample size in this preliminary investigation. Based on available published data with other IM nailing systems in synthetic bone[7], a sample size of eight samples per construct should be sufficient to detect variations in torsional stiffness greater than 13%, variations in axial stiffness greater than 5%, and variations in number of axial cycles to failure greater than 20%, at 80% power and a significance level of 0.05. Additionally, further investigation into end-of-test criterion for destructive axial testing (observed subsidence of greater than 5mm) is warranted. There is minimal justification as to the specific end-of-test parameters chosen for the given study outside of replicating prior literature[7]. Ultimately, the end-of-test criterion chosen should be reflective of clinical considerations such as risk of insult to the knee joint with construct collapse. However, it is important to note that severity reductions in the end-of-test-criterion, if justified, could serve to drastically decrease the total test time.

Due to a limited supply of titanium locking screws for which to achieve distal locking, screws were used multiple times across different constructs. As tested progressed, locking screws which had become bent from a previous test were re-used. As such, it is recommended that in future studies each titanium locking screw is used only once for testing.

With respect to the ratio of the outer diameter of the IM nails used in this study (13 mm) to the inner diameter of the femoral canal (15.5 – 16.0 mm), the next iteration of the study should seek to increase this ratio. Reducing the gap that exists between the outer wall of the IM nail and the inner wall of the femoral canal would be more reflective of current clinical practice and may increase the stability of the construct[36] by decreasing the variability of where the nail is seated with respect to the loading axis of the synthetic femur.

Finally, considering the proximal mounting fixture, the use of the Delrin mounting tube as the method of attachment for the IM nail to the load frame served to introduce inconsistencies in the angle of the construct with respect to the loading axis of the machine. Some inconsistent manufacture of the mounting tubes (via drilling) was observed, which caused slight inconsistencies in the alignment of each mounting tube with the axis of each IM nail was inconsistent. While this effect was mostly remediated through adjustment of the location of the distal mounting fixture, a more consistent manufacturing process for the mounting tubes, such as the use of a CNC lathe, is recommended to eliminate these inconsistencies in future studies. It should additionally be noted that the relatively lower modulus of Delrin as a material may have introduced undesirable compliance in the fixture assembly and should be reconsidered in the future

for studies specifically focusing on distal fixation only. A possible solution to this phenomenon and that of inconsistent manufacturing of the tubes would be the use a single stainless steel proximal mounting tube for all constructs.

Conclusion

Intraarticular fractures of the distal femur with metaphyseal comminution display lower axial stiffness and higher rates of subsidence as compared to fractures without metaphyseal comminution when fixated with retrograde IM nailing. For testing to a maximum subsidence of only 4-5 mm, it remains unclear whether this difference in construct robustness may be clinically significant and this question merits future consideration by the clinical community. For continued investigation of distal femur fractures in older adults with osteoporosis, the results of this study suggest that a 15 lb/ft^3 closed-cell polyurethane foam may be the most appropriate homogenous synthetic material to represent the distal femur. To fully address the issue of determining a representative synthetic material, however, there is a need to evaluate *in vivo* bone quality of patients who have sustained distal femur fractures, such as through computational analysis of pre-operative CT scans.

Bibliography

1. Wähnert D, Hoffmeier K, Fröber R, Hofmann GO, Mückley T. Distal femur fractures of the elderly - Different treatment options in a biomechanical comparison. *Injury*. 2011;42(7):655-659. doi:10.1016/j.injury.2010.09.009
2. Ehlinger M, Ducrot G, Adam P, Bonnomet F. Distal femur fractures. Surgical techniques and a review of the literature. *Orthop Traumatol Surg Res*. 2013;99(3):353-360. doi:10.1016/j.otsr.2012.10.014
3. Court-Brown CM, Caesar B. Epidemiology of adult fractures: A review. *Injury*. 2006;37(8):691-697. doi:10.1016/j.injury.2006.04.130
4. Beltran MJ, Gary JL, Collinge CA. Management of distal femur fractures with plates and nails. *J Orthop Trauma*. 2015;29(4):165-172. doi:10.1097/BOT.0000000000000302
5. Gangavalli AK, Nwachuku CO. Management of Distal Femur Fractures in Adults. An Overview of Options. *Orthop Clin North Am*. 2016;47(1):85-96. doi:10.1016/j.ocl.2015.08.011
6. Bonyun M, Nauth A, Egol KA, et al. Hot Topics in Biomechanically-Directed Fracture Fixation. *J Orthop Trauma*. 2014;28(4):32-35. doi:10.1097/BOT.0000000000000072
7. Wähnert D, Hoffmeier KL, von Oldenburg G, Fröber R, Hofmann GO, Mückley T. Internal Fixation of Type-C Distal Femoral Fractures in Osteoporotic Bone. *J Bone Jt Surgery-American Vol*. 2010;92(6):1442-1452. doi:10.2106/JBJS.H.01722
8. Paller DJ, Frenzen SW, Bartlett CS, Beardsley CL, Beynnon BD. A three-dimensional comparison of intramedullary nail constructs for osteopenic supracondylar femur fractures. *J Orthop Trauma*. 2013;27(2):93-99. doi:10.1097/BOT.0b013e31825199c9
9. Bliemel C, Buecking B, Mueller T, et al. Distal femoral fractures in the elderly: Biomechanical analysis of a polyaxial angle-stable locking plate versus a retrograde intramedullary nail in a human cadaveric bone model. *Arch Orthop Trauma Surg*. 2014;135(1):49-58. doi:10.1007/s00402-014-2111-8
10. Briffa N, Karthickeyan R, Jacob J, Khaleel A. Comminuted supracondylar femoral fractures: a biomechanical analysis comparing the stability of medial versus lateral plating in axial loading. *Strateg Trauma Limb Reconstr*. 2016;11(3):187-191. doi:10.1007/s11751-016-0268-0
11. Assari S, Kaufmann A, Darvish K, et al. Biomechanical comparison of locked plating and spiral blade retrograde nailing of supracondylar femur fractures. *Injury*. 2013;44(10):1340-1345. doi:10.1016/j.injury.2013.04.016
12. Mehling I, Hoehle P, Sternstein W, Blum J, Rommens PM. Nailing versus plating for comminuted fractures of the distal femur: A comparative biomechanical in vitro study of three implants. *Eur J Trauma Emerg Surg*. 2013;39(2):139-146. doi:10.1007/s00068-012-0247-1
13. Pekmezci M, McDonald E, Buckley J, Kandemir U. Retrograde intramedullary nails with distal screws locked to the nail have higher fatigue strength than locking plates in the treatment of supracondylar femoral fractures: A cadaver-based laboratory investigation. *Bone Jt J*. 2014;96 B(1):114-121. doi:10.1302/0301-620X.96B1.31135

14. Wild M, Thelen S, Spoor V, et al. Do locked compression intramedullary nails improve the biomechanical stability of distal femoral fractures? *J Trauma - Inj Infect Crit Care*. 2011;70(4):832-837. doi:10.1097/TA.0b013e3181f6f170
15. Zlowodzki M, Williamson S, Cole PA, Zardiackas LD, Kregor PJ. Biomechanical evaluation of the Less Invasive Stabilization System, angled blade plate, and retrograde intramedullary nail for the internal fixation of distal femur fractures. *J Orthop Trauma*. 2004;18(8):494-502. doi:10.1097/00005131-200409000-00004
16. Heiney JP, Barnett MD, Vrabec GA, Schoenfeld AJ, Baji A, Njus GO. Distal femoral fixation: A biomechanical comparison of trigen retrograde intramedullary (I.M.) nail, dynamic condylar screw (DCS), and locking compression plate (LCP) condylar plate. *J Trauma - Inj Infect Crit Care*. 2009;66(2):443-449. doi:10.1097/TA.0b013e31815edeb8
17. Heiner AD. Structural properties of fourth-generation composite femurs and tibias. *J Biomech*. 2008;41(15):3282-3284. doi:10.1016/j.jbiomech.2008.08.013
18. Terzidis I, Totlis T, Papathanasiou E, Sideridis A, Vlasis K, Natsis K. Gender and Side-to-Side Differences of Femoral Condyles Morphology: Osteometric Data from 360 Caucasian Dried Femori. *Anat Res Int*. 2012;2012(1):1-6. doi:10.1155/2012/679658
19. Gwathmey FW, Jones-Quaidoo SM, Kahler D, Hurwitz S, Cui Q. Distal femoral fractures: Current Concepts. *J Am Acad Orthop Surg*. 2010;18(20):597-607. doi:10.1055/s-0030-1248023
20. Schneider E, Michel MC, Genge M, Zuber K, Ganz R, Perren SM. Loads acting in an intramedullary nail during fracture healing in the human femur. *J Biomech*. 2001;34(7):849-857. doi:10.1016/S0021-9290(01)00037-9
21. Duda GN, Schneider E, Chao EYS. Internal forces and moments in the femur during walking. *J Biomech*. 1997;30(9):933-941. doi:10.1016/S0021-9290(97)00057-2
22. Dailey HL, Daly CJ, Galbraith JG, Cronin M, Harty JA. The Flexible Axial Stimulation (FAST) intramedullary nail provides interfragmentary micromotion and enhanced torsional stability. *Clin Biomech*. 2013;28(5):579-585. doi:10.1016/j.clinbiomech.2013.04.006
23. Galbraith JG, Daly CJ, Harty JA, Dailey HL. Role of the fibula in the stability of diaphyseal tibial fractures fixed by intramedullary nailing. *Clin Biomech*. 2016;38:42-49. doi:10.1016/j.clinbiomech.2016.08.007
24. ASTM. F1839 - 97: Standard Specification for Rigid Polyurethane Foam for use as a Standard Material for Testing Orthopaedic Devices and Instruments. *ASTM B Stand*. 2014;13.01(October):6-11. doi:10.1520/F1839-08R12.Copyright
25. McCalden RW, McGeough J a, Court-Brown CM. Age-related changes in the compressive strength of cancellous bone. The relative importance of changes in density and trabecular architecture. *J Bone Joint Surg Am*. 1997;79(3):421-427. doi:papers://82E9EA27-E255-4A82-9E40-6DAC45A310F4/Paper/p267
26. ASTM. Standard Test Method for Compressive Properties of Rigid Cellular Plastics 1. *ASTM B Stand*. 2016:4-8. doi:10.1520/D1621-16.2
27. ASTM. Standard Test Method for Apparent Density of Rigid Cellular Plastics. *ASTM B Stand*. 2003;82(Reapproved):3-6. doi:10.1520/D1622-14.2
28. Graichen F, Schwachmeyer V, Damm P, Bender A, Bergmann G. In Vivo Hip

Joint Loading during Post-Operative Physiotherapeutic Exercises. 2013;8(10):12-14. doi:10.1371/journal.pone.0077807
29. Heiner AD, Brown TD. Structural properties of a new design of composite replicate femurs and tibias. *J Biomech*. 2001;34(6):773-781. doi:10.1016/S0021-9290(01)00015-X
30. Wähnert D, Hoffmeier KL, Stolarczyk Y, Fröber R, Hofmann GO, Mückley T. Evaluation of a customized artificial osteoporotic bone model of the distal femur. *J Biomater Appl*. 2011;26(4):451-464. doi:10.1177/0885328210367830
31. Linde F, Hvid I, Pongsoipetch B. Energy absorptive properties of human trabecular bone specimens during axial compression. *J Orthop Res*. 1989;7(3):432-439. doi:10.1002/jor.1100070316
32. Carter DR, Hayes WC. The Compressive Behavior Porous of Bone Structure as a Two-Phase. *J bone Jt Surg*. 1977;59(7):954-962. doi:10.1007/978-1-4471-5451-8_116
33. Galante J, Rostoker W, Ray RD. Physical properties of trabecular bone. *Calcif Tissue Res*. 1970;5(1):236-246. doi:10.1007/BF02017552
34. Goldstein SA, Wilson DL, Sonstegard DA, Matthews LS. The mechanical properties of human tibial trabecular bone as a function of metaphyseal location. *J Biomech*. 1983;16(12):965-969. doi:10.1016/0021-9290(83)90097-0
35. Gibson LJ. The mechanical behaviour of cancellous bone. *J Biomech*. 1985;18(5):317-328. doi:10.1016/0021-9290(85)90287-8
36. Mahar A, Sink E, Faro F, Oka R, Newton PO. Differences in biomechanical stability of femur fracture fixation when using titanium nails of increasing diameter. *J Child Orthop*. 2007;1(3):211-215. doi:10.1007/s11832-007-0040-6

Appendix

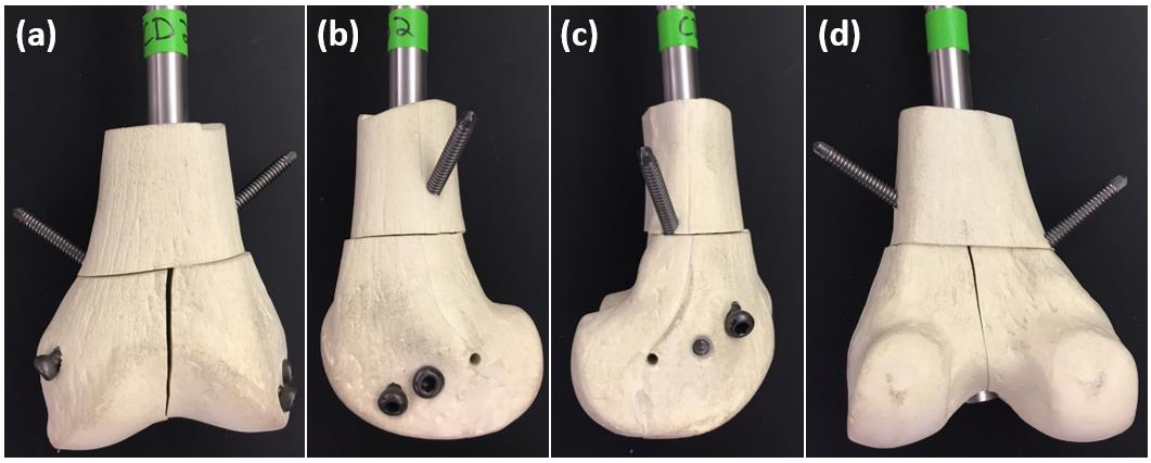

Figure 1: Images of NC1 construct prior to mechanical testing. From left to right, (a) Anterior, (b) Lateral, (c) Medial, (d) Posterior.

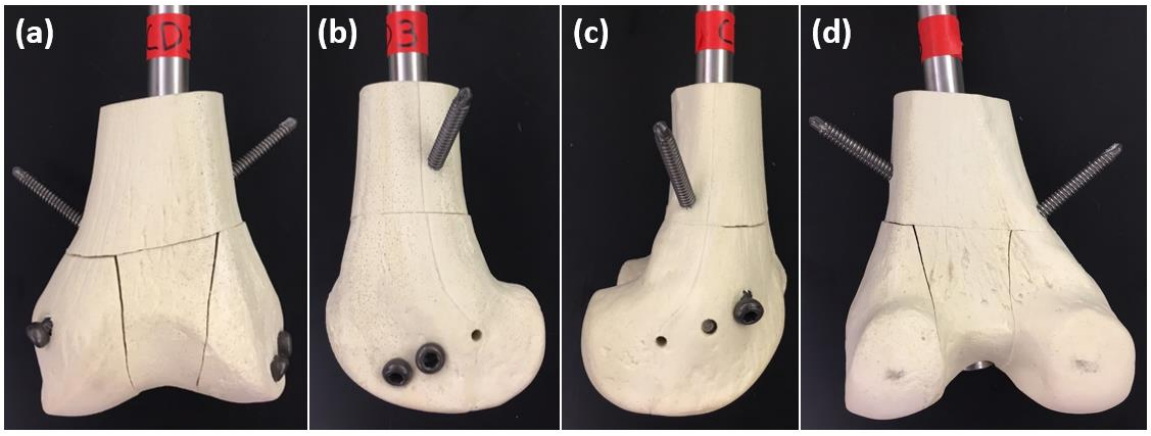

Figure 2: Images of C2 construct prior to mechanical testing. From left to right, (a) Anterior, (b) Lateral, (c) Medial, (d) Posterior.

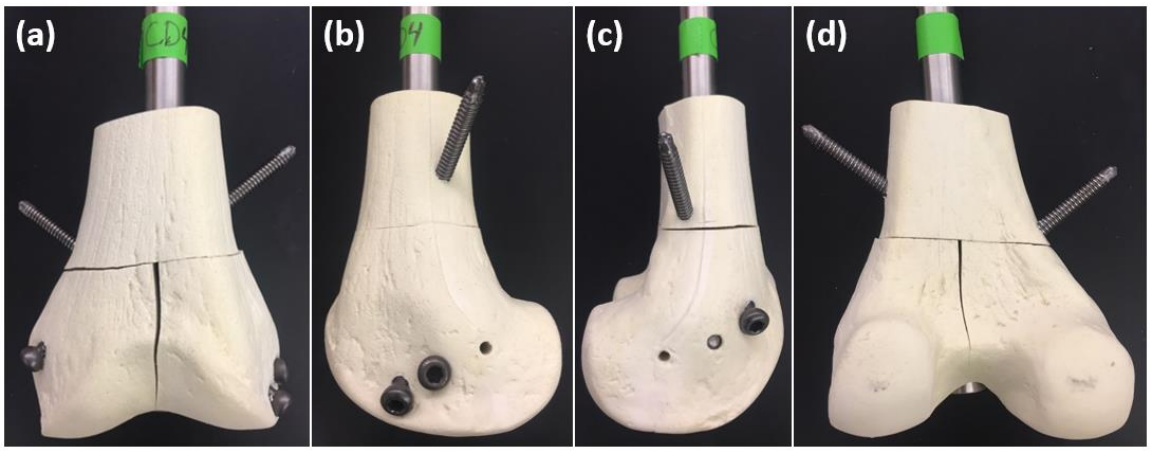

Figure 3: Images of NC2 construct prior to mechanical testing. From left to right, (a) Anterior, (b) Lateral, (c) Medial, (d) Posterior.

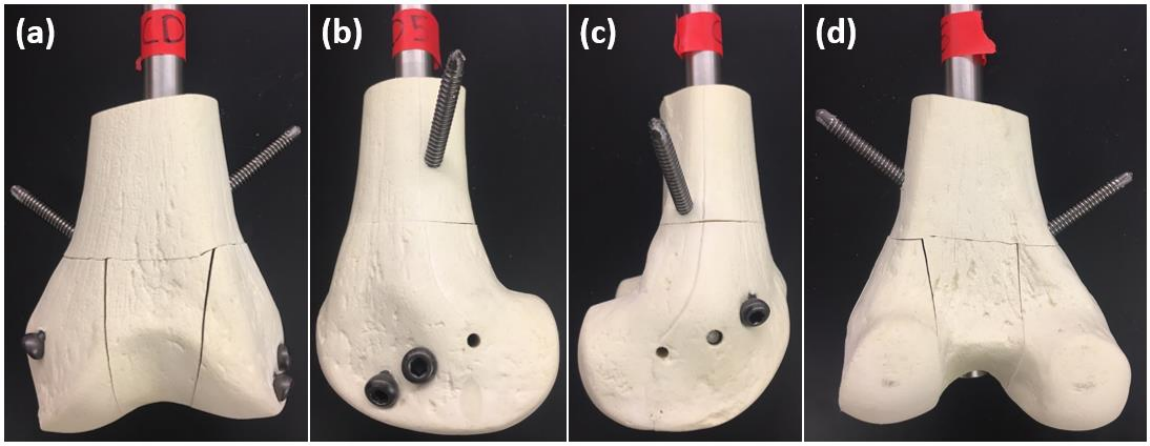

Figure 4: Images of C5 construct prior to mechanical testing. From left to right, (a) Anterior, (b) Lateral, (c) Medial, (d) Posterior.

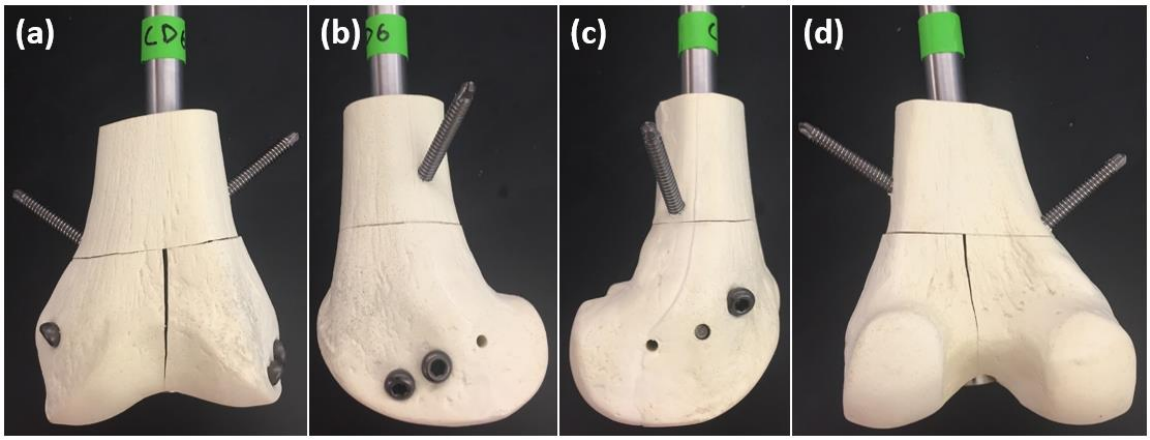

Figure 5: Images of NC3 construct prior to mechanical testing. From left to right, (a) Anterior, (b) Lateral, (c) Medial, (d) Posterior.

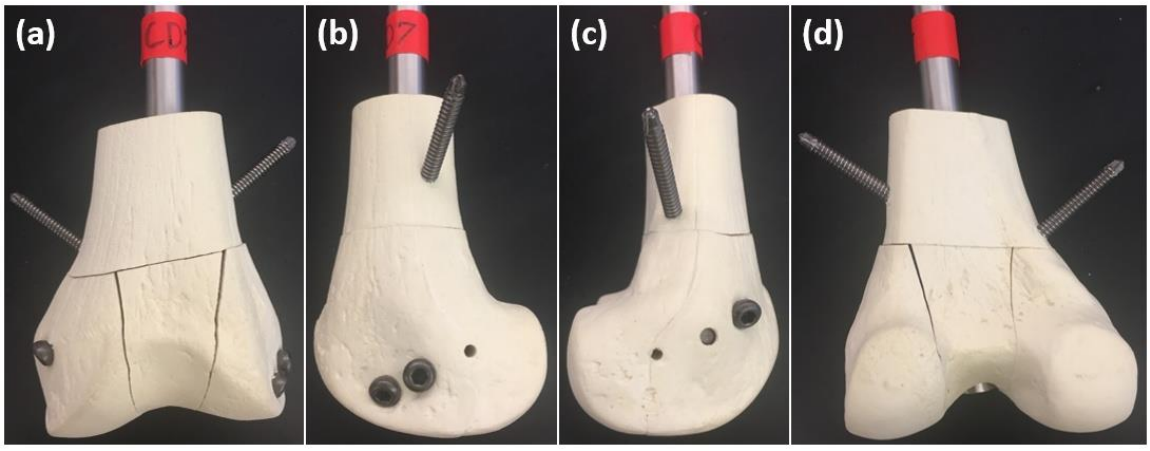

Figure 6: Images of C3 construct prior to mechanical testing. From left to right, (a) Anterior, (b) Lateral, (c) Medial, (d) Posterior.

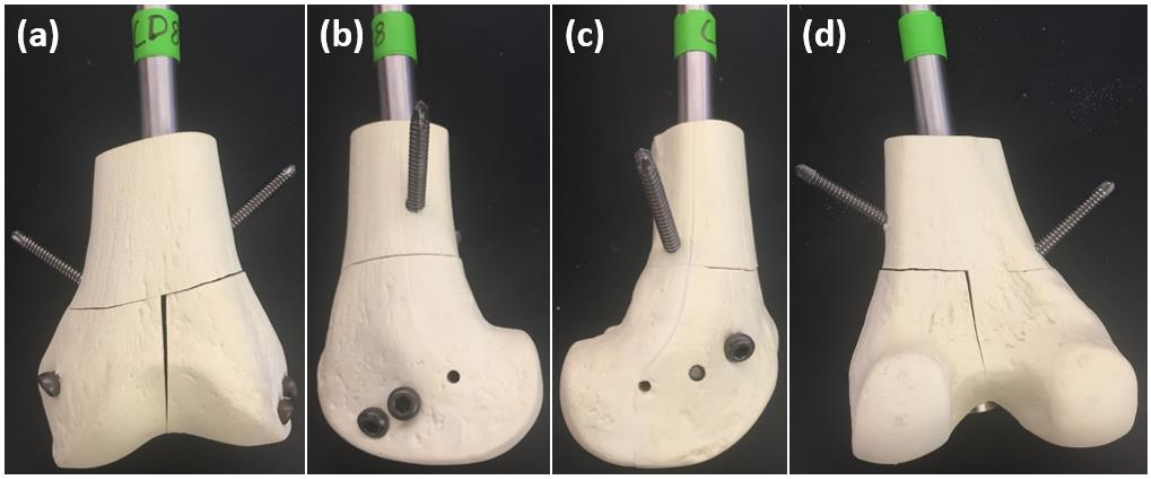

Figure 7: Images of NC4 construct prior to mechanical testing. From left to right, (a) Anterior, (b) Lateral, (c) Medial, (d) Posterior.

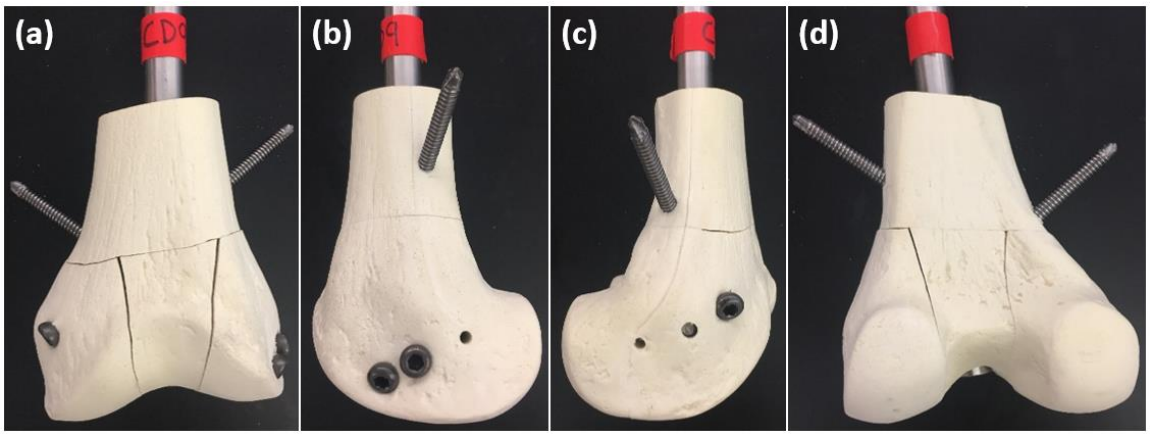

Figure 8: Images of C4 construct prior to mechanical testing. From left to right, (a) Anterior, (b) Lateral, (c) Medial, (d) Posterior.

Vita of Christian T. Davis

Birth

- Born October 23, 1994 in Beverly, Massachusetts to Lincoln and Kristin Davis

Education

- B.S. in Mechanical Engineering, Lehigh University, 2013-2017